CRS4

Centre for Advanced Studies,
Research and Development in Sardinia
Uta - (CA)

Programma ENEA-MURST

Obiettivo 8

Development of a non-adiabatic premixed model into the Ares combustion code

by:

M. Talice and M. Mulas
Computational Fluid Dynamics Area

Contents

Abstract

The present report somehow represents the summa of the activities which have been carried out during the third and conclusive year of the project. In [3] the necessity of modifying the original goal of the present task, has emerged. In fact, the research work carried out in [3] has shown that the original adiabatic formulation of the TFC model was not sufficient to achieve a qualitatively and quantitatively fair description of the fluid dynamic fields (velocity and temperature) inside a combustion chamber whenever the energy diffusion phenomena cannot be neglected, which is the case in the actual industrial burners.

In the same report [3] it was discussed the how the TFC model formulation could be modified in order to take into account the diffusion of thermal energy, and the non adiabatic version of the TFC model available in the code Fluent was tested against the ENSMA experimental combustor test case [1]. The obtained results were such to make advisable to reformulate the original conclusive task of the project in order to implement the non adiabatic version of the TFC model into the code Ares.

In Chapter 1 a brief summary of the model will be presented. Interested readers could find a more detailed description in [3] or in [2]. In Chapter 2 the validation of the model against the ENSMA combustor will be illustrated. Both the adiabatic and non adiabatic TFC models have been used, and the calculation has been repeated by using all the two-equations turbulence models which are available in Ares, namely the Standard and RNG $\kappa - \epsilon$ models and the $\kappa - log(\omega)$ version of the Wilcox model. The Spalart & Allmaras one-equation turbulence model, which is also available in Ares, has not been used here for its intrinsic limitation in dealing with given profiles of the turbulent quantities at the inlet section.

1 Non-adiabatic TFC Equations

An accurate description of the TFC adiabatic formulation can be found in [5] and [4]. The final model equation writes as:

$$\frac{\partial(\overline{\rho}\tilde{c})}{\partial t} + \frac{\partial(\overline{\rho}\tilde{u}_i\tilde{c})}{\partial x_i} = \frac{\partial}{\partial x_i}\left(\overline{\rho}D_t\frac{\partial\tilde{c}}{\partial x_i}\right) + \rho\dot{W} \quad (1)$$

The progress variable source term $\rho\dot{W}$ which appeares in equation 1 is modeled as:

$$\rho\dot{W} = U_t\,\rho_u\,|\nabla c| = A\,G u'^{\{\frac{3}{4}\}} U_l^{\{\frac{1}{2}\}} \chi^{\{-\frac{1}{4}\}} \ell_t^{\{\frac{1}{4}\}} \rho_u\,|\nabla c| \quad (2)$$

Where the turbulent velocity fluctuation u' and the turbulent lenght scale ℓ_t can be expressed as functions of the turbulent kinetic energy and its dissipation rate. Their actual formulation depends on the choosen turbulent model.

The expression of the stretch factor G which appeares in equation 2 can be found again in [5] and [4].

In the adiabatic TFC model, the energy equation is not solved and it is de facto replaced by the progress variable equation, only. Thus temperature is computed at post-processing stage as:

$$\overline{T} = T_b\,\tilde{c} + (1-\tilde{c}) * T_u$$

The mathematical model is closed by adding an extra constitutive relation, namely an appropriate equation of state. By using the uncompressible form of the ideal gas law, density can be computed as:

$$\overline{\rho} = \frac{\rho_u T_u}{\overline{T}} \quad (3)$$

Equation 3, by writing the temperature $\overline{T}$ according to equation 1, becomes:

$$\overline{\rho} = \frac{\rho_u T_u}{T_b\,\tilde{c} + \left(1-\tilde{c}\right) * T_u}$$

After some algebra, the final expression for the computation of density, becomes:

$$\overline{\rho} = \frac{1}{\tilde{c}/\rho_b + (1-\tilde{c})T_u} \quad (4)$$

Equations 1 and 4 put in evidence how temperature or density depend on the progress variable field only, and no possibility exists in the model to exchange thermal energy between fluid regions at different temperature levels.

For the non-adiabatic model, the solution of the energy transport equation is needed in order to compute the actual temperature distribution. Combustion is accounted for by the introduction of a suitable source term for the enthalpy. Thus, energy equation in terms of enthalpy writes as:

$$\frac{\partial}{\partial t}(\overline{\rho}\widetilde{h}) + \frac{\partial}{\partial x_i}(\overline{\rho}\widetilde{u}_i\widetilde{h}) = \frac{\partial}{\partial x_i}\left(\frac{\kappa + \kappa_t}{c_p}\frac{\partial}{\partial x_i}\widetilde{h}\right) + S_{h,chem} \tag{5}$$

where $S_{h,chem}$ represents the enthalpy source term due to the chemical reactions. In the non adiabatic TFC formulation, $S_{h,chem}$ is modeled as:

$$S_{h,chem} = \rho\dot{W} H_{comb} m_f \tag{6}$$

being:

- $\rho\dot{W}$ the average specific product formation date;
- H_{comb} the heat of combustion for burning 1 kg of fuel;
- m_f the fuel mass fraction of unburnt mixture

The term $\rho\dot{W}$ is computed according to expression 2.
The temperature can be computed from the enthalpy equation 5 by:

$$\overline{T} = \frac{\widetilde{h}}{c_p} \tag{7}$$

and can be introduced in equation 3 to compute the density field.

2 Test case description

The experimental set-up is shown in figure 1, where a longitudinal section of the combustion chamber is represented.

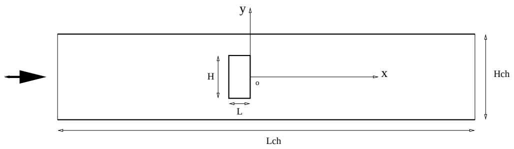

Figure 1: Test Case Geometry.

A premixed mixture of propane and air flows through a channel, where a square section bar has been inserted. The channel and obstacle dimensions are those reported in table 1

Channel			Obstacle		
$L_{\{ch\}}(mm)$	$H_{\{ch\}}(mm)$	$W_{\{ch\}}(mm)$	$L\ (mm)$	$H\ (mm)$	$W\ (mm)$
2200	28.8	160	5	9.6	160

Table 1: Geometric dimension

For a hydrocarbon fuel given by $C_{\{x\}}H_{\{y\}}$, the stoichiometric reaction can be written as:

$$C_xH_y + a\,(O_2 + 3.76N_2) \;\rightarrow\; xCO_2 + (y/2)H_2O + 3.76aN_2$$

where: $a = x + y/4$.

The stoichiometric air to fuel ratio is given by:

$$(A/F)_{\{stoic\}} = \left(\frac{m_{air}}{m_{fuel}}\right) = \frac{4.76a}{1}\frac{MW_{air}}{MW_{fuel}}$$

where $MW_{air}$and $MW_{fuel}$are the molecular weight of air and fuel, respectively.

The temperature of the mixture at the inlet section is $273K$ and the mass-flow per unit of channel thickness is equal to $0.2722\,Kg/m/s$, corresponding to a maximum speed of the main flow of $8.2\,m/s$. The resulting Reynolds number based on the channel height is $Re = 17810$, whereas the corresponding value based on the obstacle height is $Re = 5937$.

The chemical reaction which describes the combustion process is given by:

equivalence ratio	Φ	0.65
fuel mass fraction	$Y_{C_3H_8}$	0.04
oxygen mass fraction	Y_{O_2}	0.2237
nitrogen mass fraction	Y_{N_2}	0.7363
mixture temperature	T_{unb}	273.0
adiabatic flame temperature	T_{adiab}	1780.0
mixture density	ρ_{unb}	1.3059
heat of combustion	H_{comb}[J/Kg]	50.0
specific heat	C_P	1614

Table 2: Mixture composition and properties

$$\Phi C_3H_8 + 5(O_2 + 3.76N_2) \rightarrow \Phi CO_2 + 4\Phi H_2O + (5 - 5\Phi)O_2 + 18.8N_2$$

The mixture composition together with other quantities of interest are reported in table 2, where the mixture equivalence ratio is defined as:

$$\Phi = \frac{(A/F)_{stoic}}{(A/F)}$$

Measurements are available for non-reactive and reactive flow conditions and the description of the experimental results can be found in reference [1]. The experiments have found the evidence of the existence of two vortexes downstream the obstacle. The effect of this recirculation zone is the stabilization of the flame. The longitudinal extension of the recirculation zone has been measured to be equal to $4x/H$ along the combustor axis.

2.1 Numerical simulation

Figure 2 shows the grid topology of the 4-block mesh used, and an enlargement of the computational domain around the obstacle. In the same figure, the positions of the three cross-sections on which experimental data are available, are also shown. In order to assure grid independence results, the computations have been repeated by using two finer meshes which are obtained by doubling the number of cells of the coarse grid. Table 3 gives the number of cells used in the x and y directions for each block and for each grid level. Results obtained with grid level B de facto match those obtained with grid level C, and will be the only ones reported in the following.

As previously mentioned, the stabilization of the flame behind the flame holder is due to the presence of two vortexes. Hence, a correct description of the turbulent flow behavior is a critical issue of the test case simulation. The turbulence models which have been used were the two models of the $\kappa - \epsilon$ family, namely standard and RNG, plus the $\kappa - log(\omega)$ model. The Spalart and Allmaras one-equation turbulence model which has been implemented into the ARES code, has not been used in the simulation. In fact, an intrinsic limitation of that model is that it is not possible to clearly assign to the incoming flow a chosen turbulence intensity (or a given profile of turbulent kinetic energy). The validation of the model is hence postponed to a successive task.

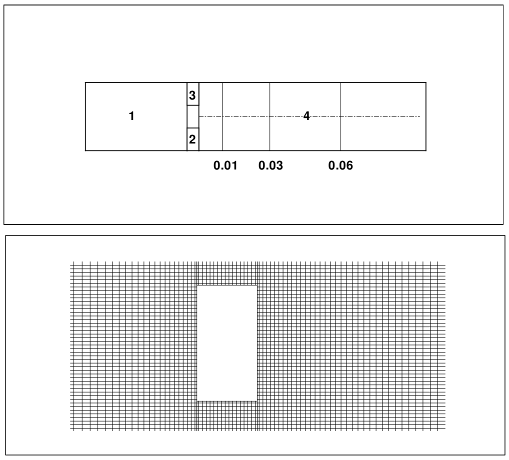

Figure 2: Blocks topology (up); mesh detail around the obstacle (bottom)

Inlet profiles (transversal distributions) for the average quantities $\overline{u}, \overline{\kappa}$ and $\overline{\varepsilon}$ have been imposed at the inlet section and are those reported in figures 4 and 5. The value of $\overline{\kappa}$ and $\overline{\varepsilon}$ have been computed from the measured profiles of $\sqrt{u'^2}$ and $\sqrt{v'^2}$ by using relations:

$$\kappa = \frac{1}{2}\left(\sqrt{u'^2} + 2. * \sqrt{v'^2}\right) \; ; \qquad \varepsilon = -c_\mu \frac{\kappa^2}{\overline{uv}} \frac{\partial \overline{u}}{\partial y}$$

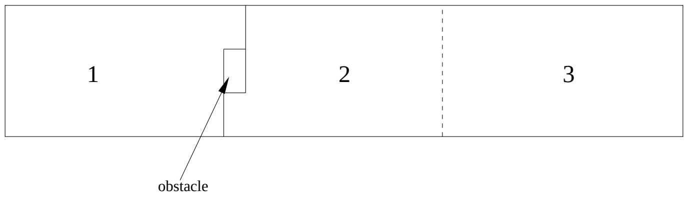

Figure 3: Domain splitting for the ARES parallel calculation

	Level A			Level B			Level C		
BI	NI	NJ	Cells	NI	NJ	Cells	NI	NJ	Cells
1	48	96	4608	96	192	18432	192	384	73728
2	32	64	2048	64	128	8192	128	256	32768
3	32	64	2048	64	128	8192	128	256	32768
4	96	96	9216	192	192	36864	384	384	147456
			17920			71680			286720

Table 3: Mesh size

In the case of the $\kappa - log(\omega)$ model, the $log(\omega)$ profile has been imposed at the inlet section. It can been computed from the corresponding κ and ϵ ones by using the relation:

$$log(\omega) = \frac{\epsilon}{c_\mu \kappa}$$

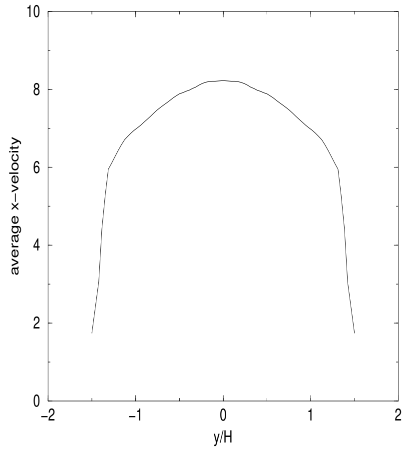

Figure 4: x-velocity distrinution at inlet

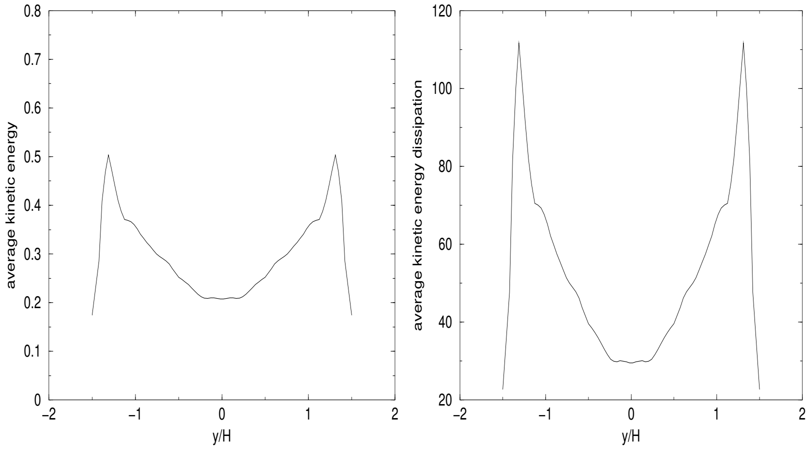

Figure 5: κ and ϵ

Wall functions have been used at solid walls for the $\kappa - \epsilon$ family calculation, whereas turbulent quantities have been integrated down to solid walls in the $\kappa - log(\omega)$ case. At the outlet section, the pressure value of 101325 [Pa] has been imposed. Isothermal conditions have been imposed at solid walls. The incoming flow temperature value has been set to 273 K. Both the adiabatic and non adiabatic versions of the TFC premixed combustion model have been used for the present computation. An exhaustive description of the adiabatic model could be found in [5] and [4].

The inlet value of the progress variable $\tilde{c}$ has been set to zero (unburned mixture). For the adiabatic calculation the value of the burned mixture density has been set to $\rho_{bnd} = 0.20$.

In the non adiabatic case isothermal conditions have been used at solid walls. The temperature of the channel walls have been set to 273 K, whereas the obstacle walls temperature, accordingly to the results already obtained in [3], was set to 600 K.

The QUICK spatial discretization scheme has been used, and the linear system was integrated by making use of the BICGSTAB, preconditioned by the ADI algorithm.

2.2 Results

The figures 6, 7 and 8 show the comparison of the computed temperature profiles to the experimental data at $x/H = 1.04167$, $x/H = 3.125$ and $x/H = 6.25$ from the obstacle. The maximum value of the temperature which has been computed by using the adiabatic TFC model is equal to the adiabatic flame temperature of the mixture, namely 1780 K. In fact it ought to be recalled here that by using the adiabatic model, temperature is computed at a post-processing stage as a function of the progress variable $\tilde{c}$ as:

$$T = T_{adiab}\tilde{c} + T_{unb}(1 - \tilde{c})$$

From the exam of figures 6, 7 and 8 it can be seen that the error committed in the evaluation of the temperature at the first considered cross section, reduces from some 500 K to nearly 150 K. At the two stations further downstream the combustor chamber, the maximum value of temperature is well captured by the non adiabatic model, whereas the error which is made by using the adiabatic model is still of about 280 K.

Figure 10 shows the velocity streamlines over the progress variable contour plot background, for the non adiabatic computation. Analysis of the figure show the influence of the different turbulence models on the ricirculation region lenght. The quantitative evaluation of the ricirculation region amplitude can be retrieved from the figure 9, which shows the comparison of the streamwise velocity component to the experimental data.

Profiles of the streamwise and crosswise components of the velocity are shown in figures 11, 12, 13 and 14, 15, 16 respectively.

The figure 17 shows the computed turbulent kinetic energy distribution at the first cross section from the obstacle.

The exam of figures from 18 to 28 allows to compare the computed results in dependence on the turbulence model which has been used for the computation.

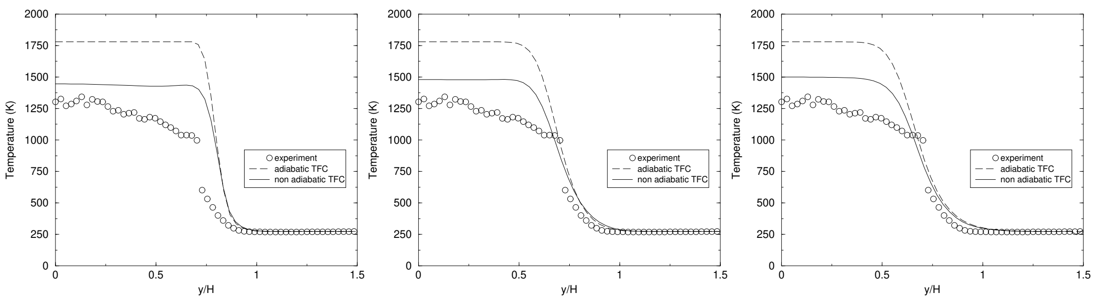

Figure 6: temperature distribution at $x/H = 1.04167$: RNG $\kappa - \epsilon$ (left); Std $\kappa - \epsilon$ (middle); $\kappa - log(\omega)$ (right);

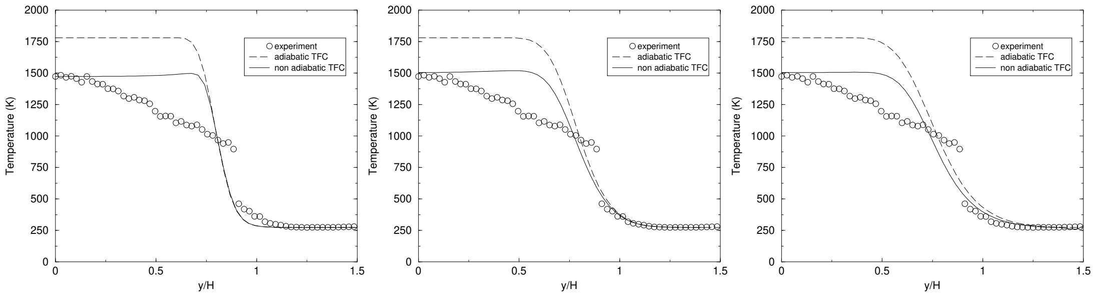

Figure 7: temperature distribution at $x/H = 3.125$: RNG $\kappa - \epsilon$ (left); Std $\kappa - \epsilon$ (middle); $\kappa - log(\omega)$ (right);

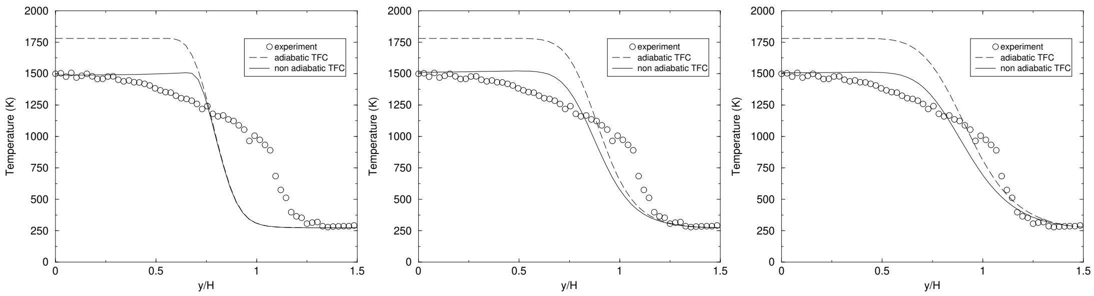

Figure 8: temperature distribution at $x/H = 6.25$: RNG $\kappa - \epsilon$ (left); Std $\kappa - \epsilon$ (middle); $\kappa - log(\omega)$ (right);

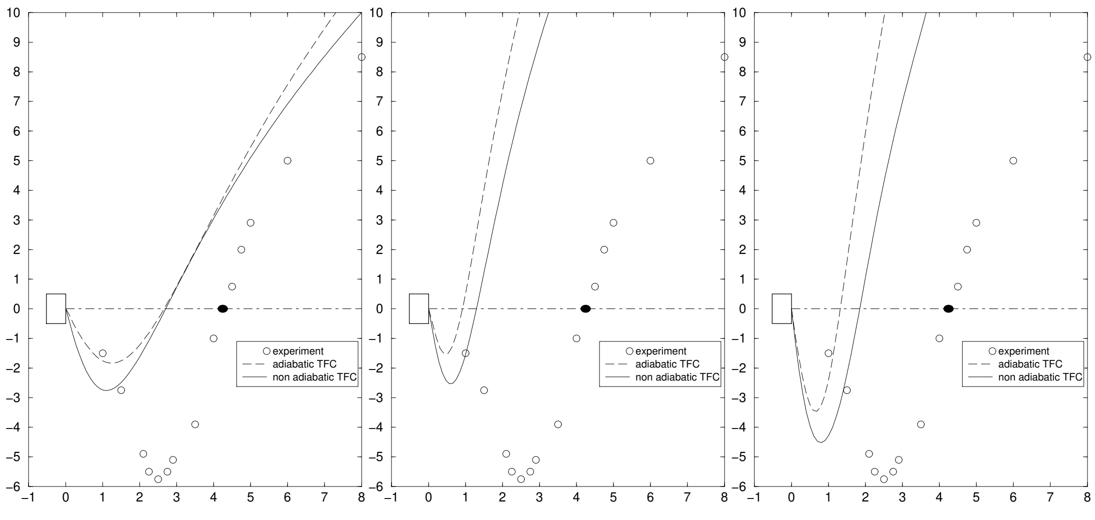

Figure 9: x-velocity distribution along the combustor axis: RNG $\kappa - \epsilon$ (left); Std $\kappa - \epsilon$ (middle); $\kappa - log(\omega)$ (right);

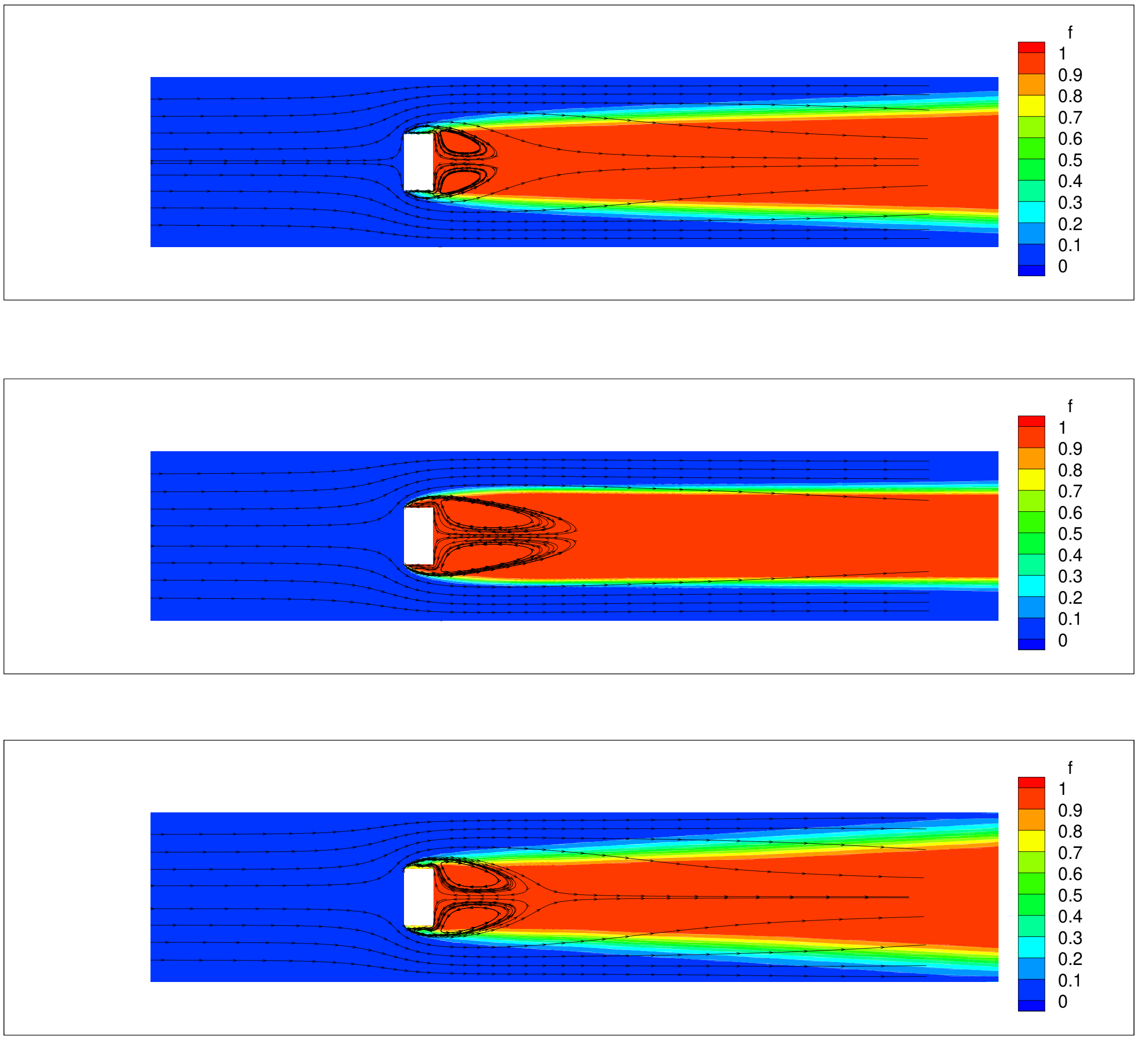

Figure 10: Streamlines over progress variable contour: Standard $\kappa - \epsilon$ (top); RNG $\kappa - \epsilon$ (middle); $\kappa - log(\omega)$ (bottom);

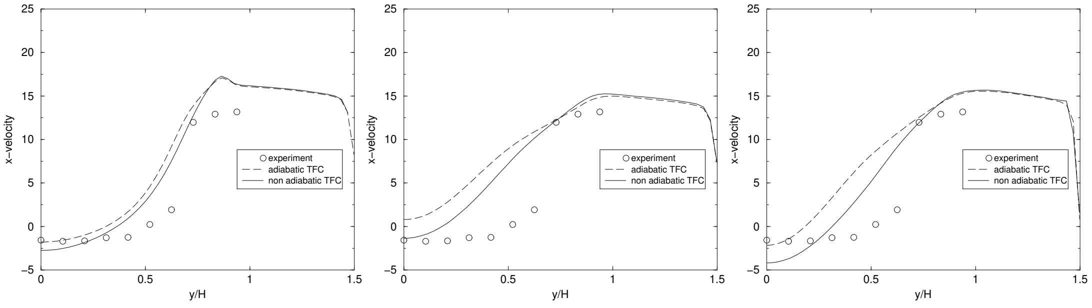

Figure 11: x-velocity distribution at $x/H = 1.04167$: RNG $\kappa - \epsilon$ (left); Std $\kappa - \epsilon$ (middle); $\kappa - log(\omega)$ (right).;

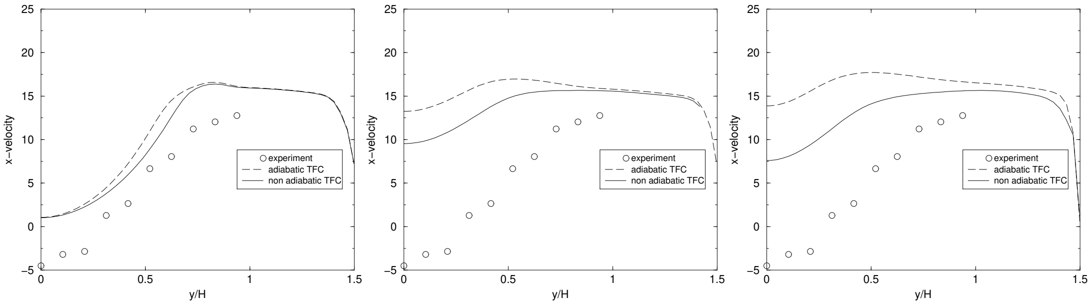

Figure 12: x-velocity distribution at $x/H = 3.125$: RNG $\kappa - \epsilon$ (left); Std $\kappa - \epsilon$ (middle); $\kappa - log(\omega)$ (right);

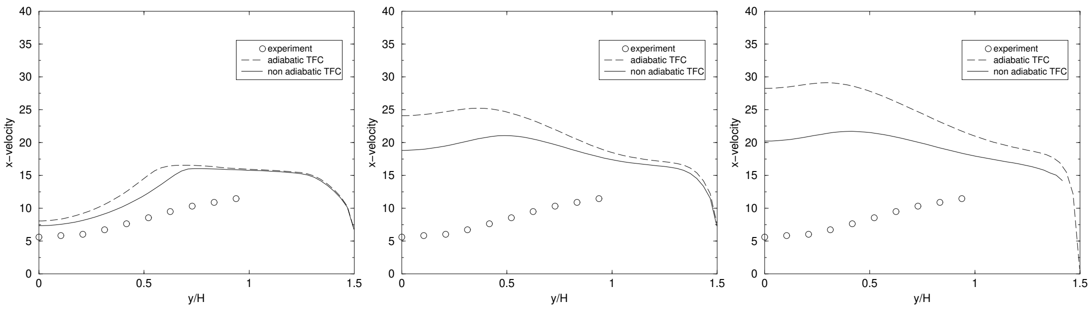

Figure 13: x-velocity distribution at $x/H = 6.25$: RNG $\kappa - \epsilon$ (left); Std $\kappa - \epsilon$ (middle); $\kappa - log(\omega)$ (right);

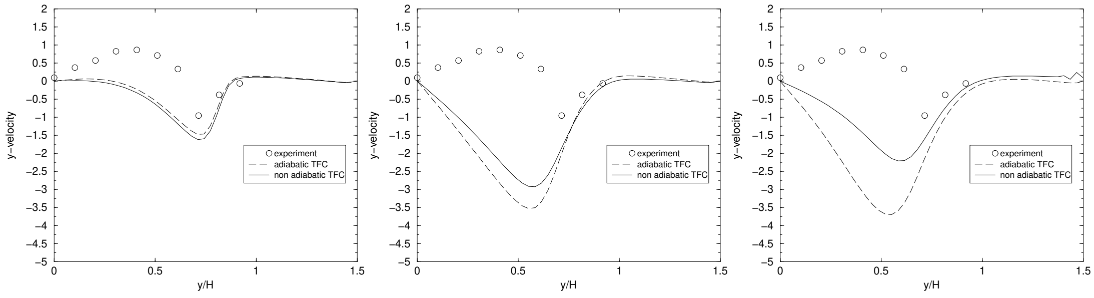

Figure 14: y-velocity distribution at $x/H = 1.04167$: RNG $\kappa - \epsilon$ (left); Std $\kappa - \epsilon$ (middle); $\kappa - log(\omega)$ (right);

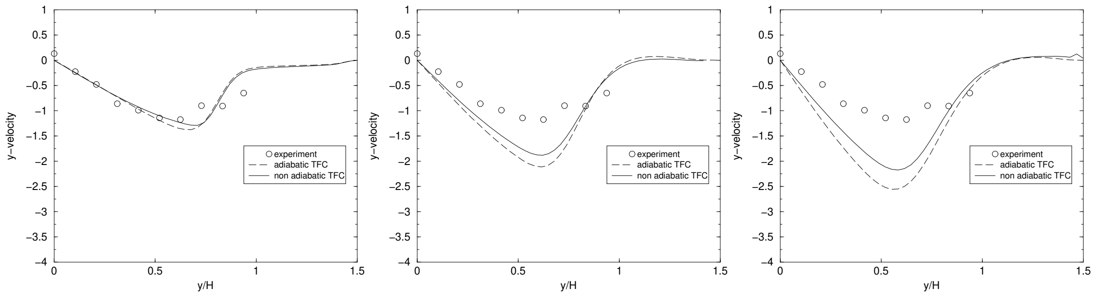

Figure 15: y-velocity distribution at $x/H = 3.125$: RNG $\kappa - \epsilon$ (left); Std $\kappa - \epsilon$ (middle); $\kappa - log(\omega)$ (right);

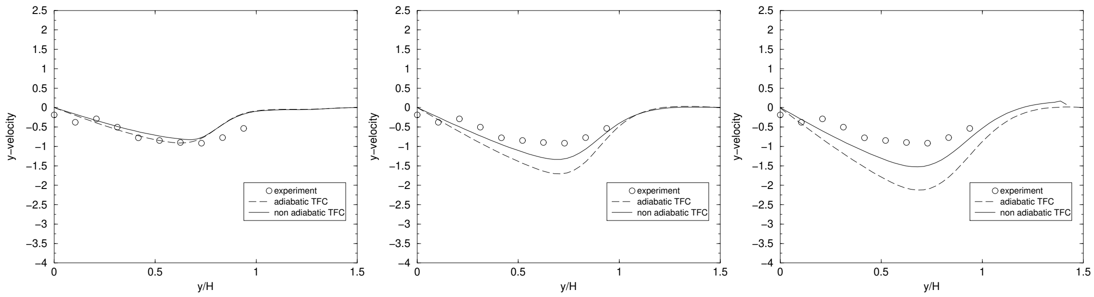

Figure 16: y-velocity distribution at $x/H = 6.25$: RNG $\kappa - \epsilon$ (left); Std $\kappa - \epsilon$ (middle); $\kappa - log(\omega)$ (right);

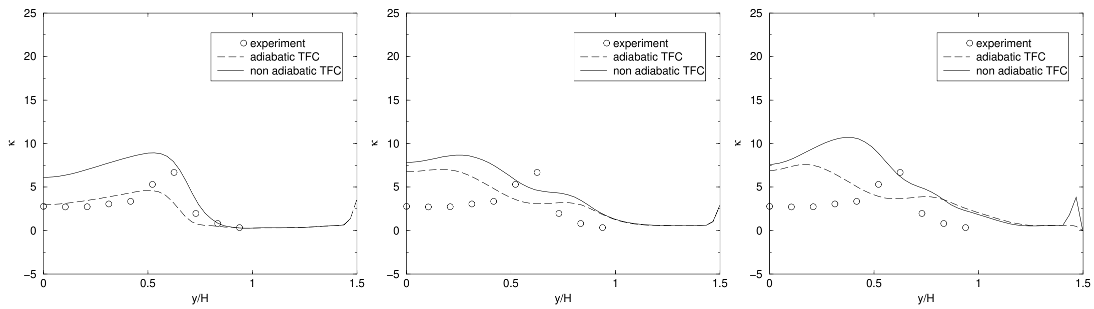

Figure 17: turbulent kinetic energy distribution at $x/H = 1.04167$: RNG $\kappa-\epsilon$ (left); Std $\kappa-\epsilon$ (middle); $\kappa - log(\omega)$ (right).

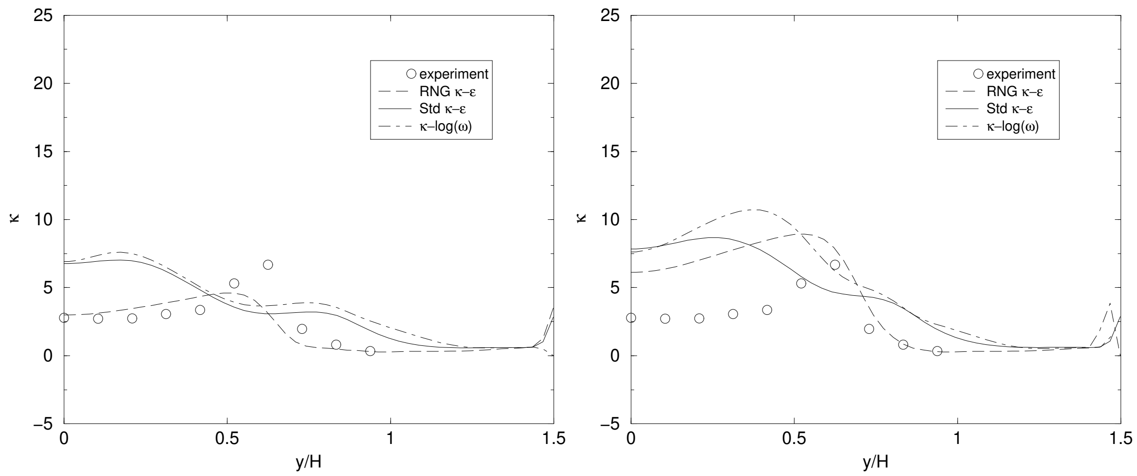

Figure 18: turbulent kinetic energy distribution at $x/H = 1.04167$: adiabatic model (left); non adiabatic model (right);

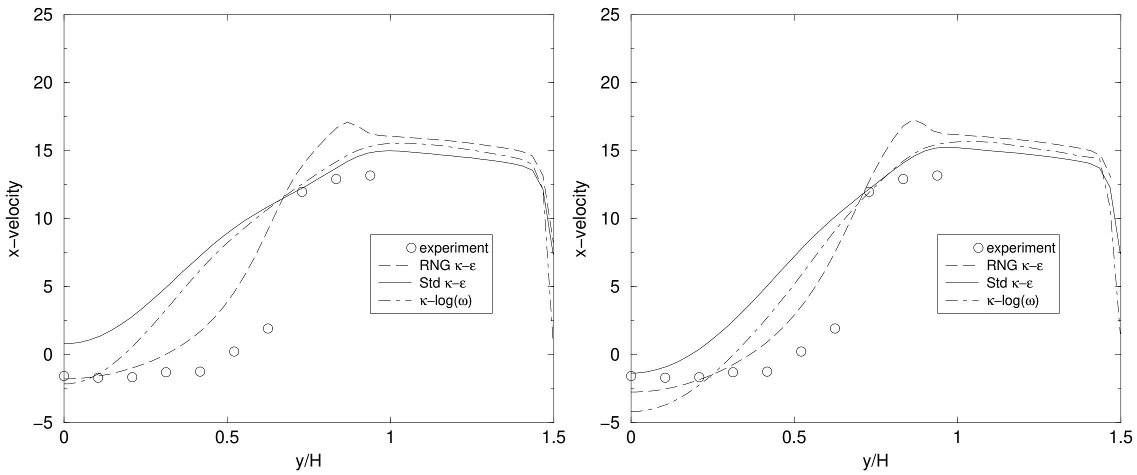

Figure 19: x-velocity distribution at $x/H = 1.04167$: adiabatic model (left); non adiabatic model (right);

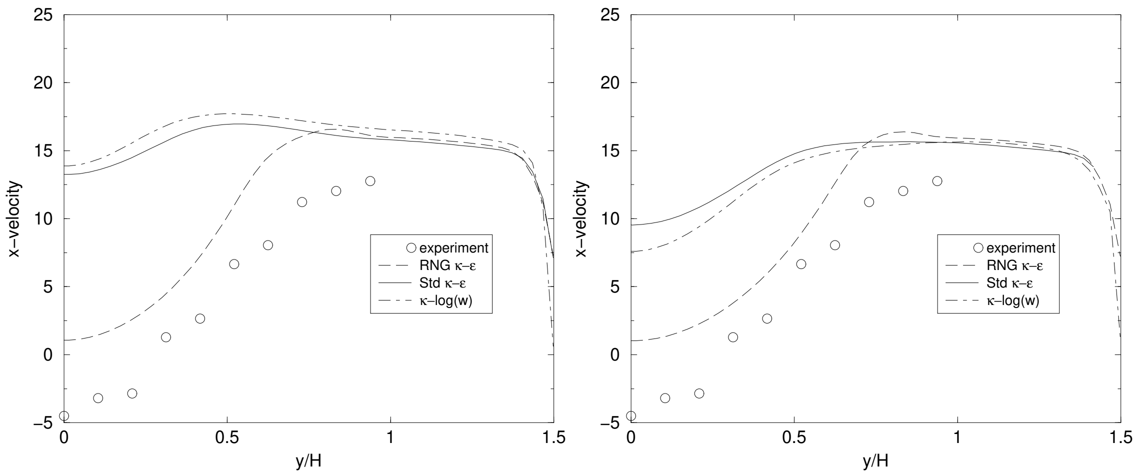

Figure 20: x-velocity distribution at $x/H = 3.125$: adiabatic model (left); non adiabatic model (right);

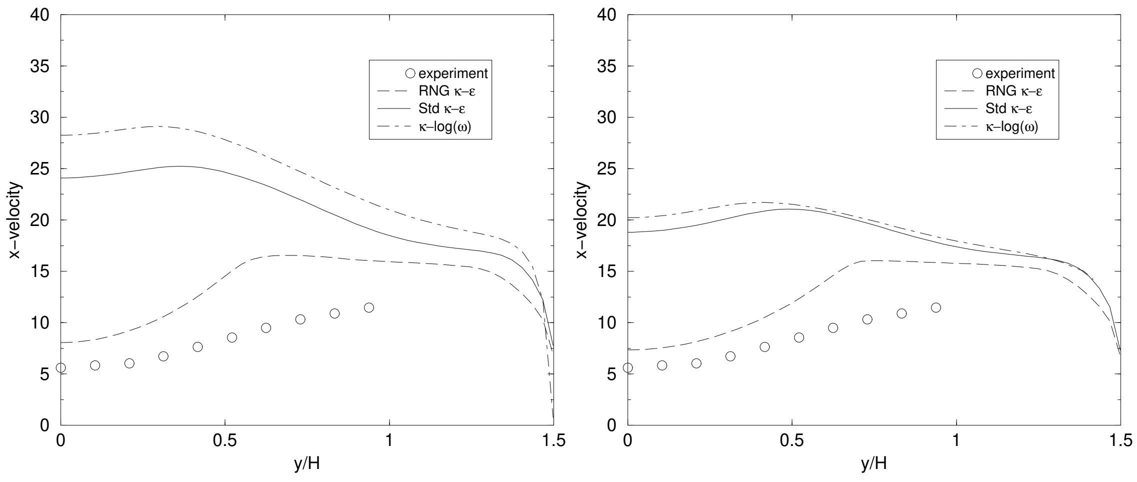

Figure 21: x-velocity distribution at $x/H = 6.25$: adiabatic model (left); non adiabatic model (right);

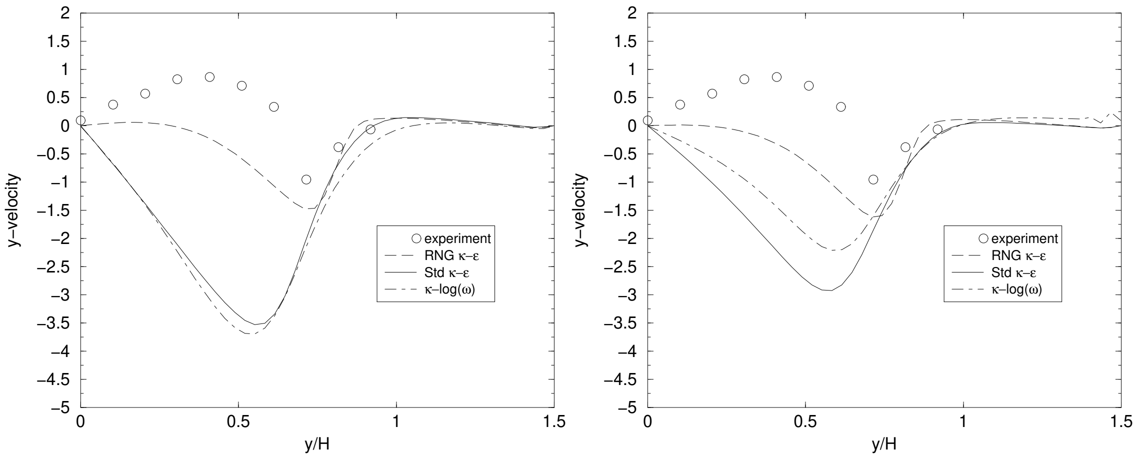

Figure 22: y-velocity distribution at $x/H = 1.04167$: adiabatic model (left); non adiabatic model (right);

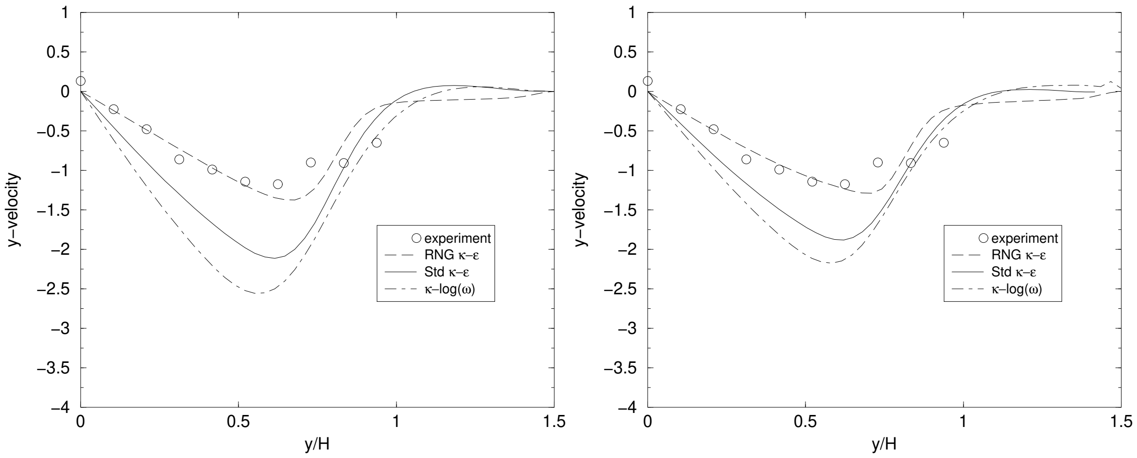

Figure 23: y-velocity distribution at $x/H = 3.125$: adiabatic model (left); non adiabatic model (right);

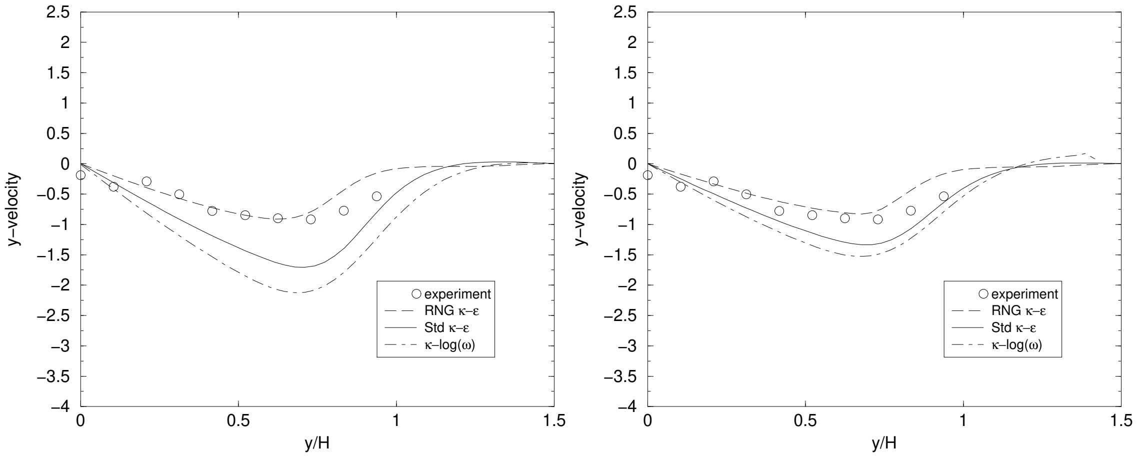

Figure 24: y-velocity distribution at $x/H = 6.25$: adiabatic model (left); non adiabatic model (right);

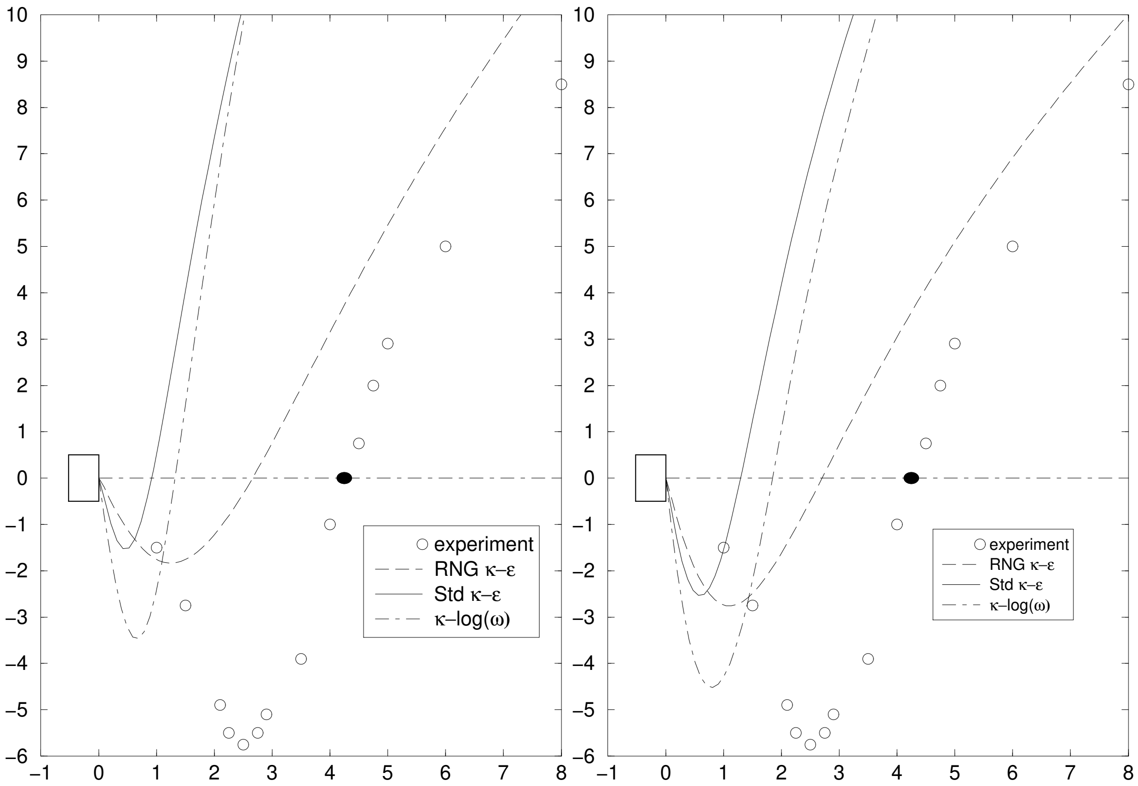

Figure 25: x-velocity distribution along the combustor axis: adiabatic model (left); non adiabatic model (right);

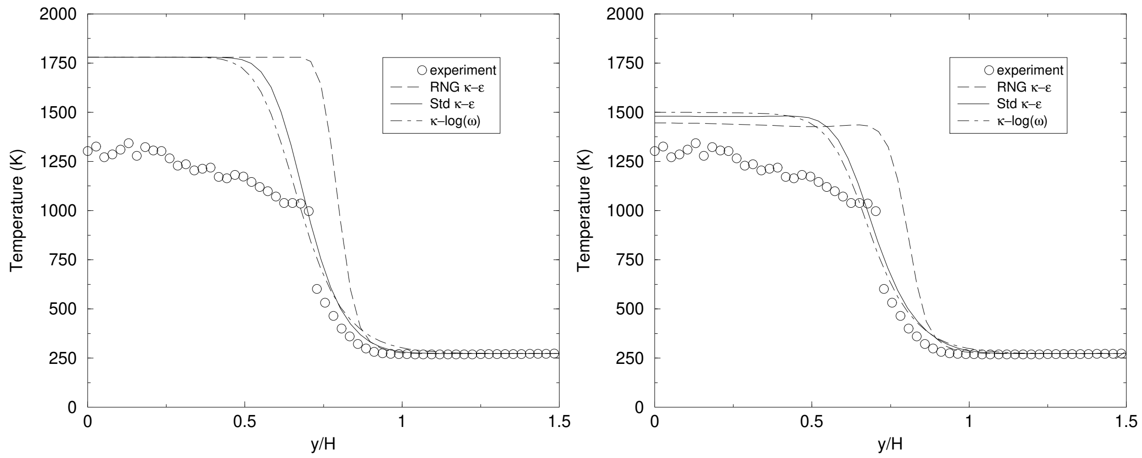

Figure 26: temperature distribution at $x/H = 1.04167$: adiabatic model (left); non adiabatic model (right);

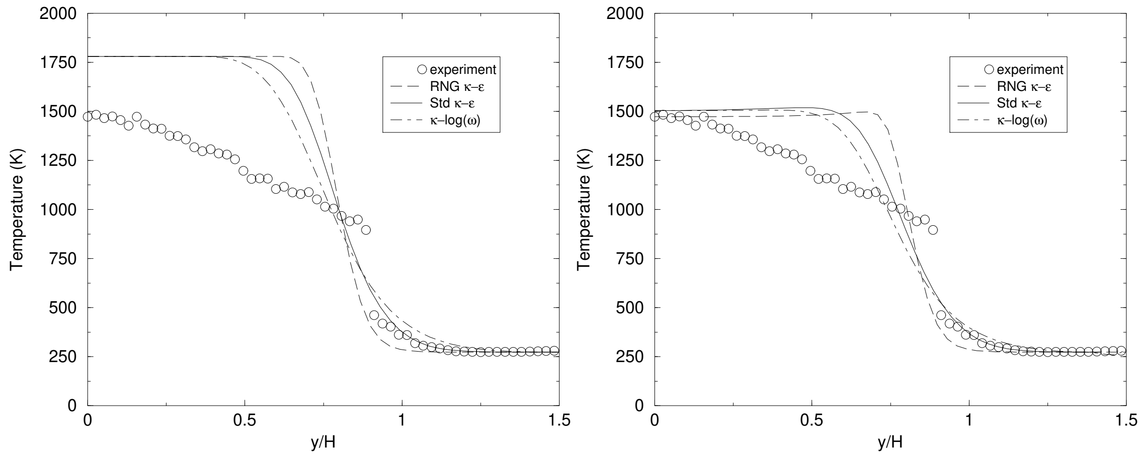

Figure 27: temperature distribution at $x/H = 3.125$: adiabatic model (left); non adiabatic model (right);

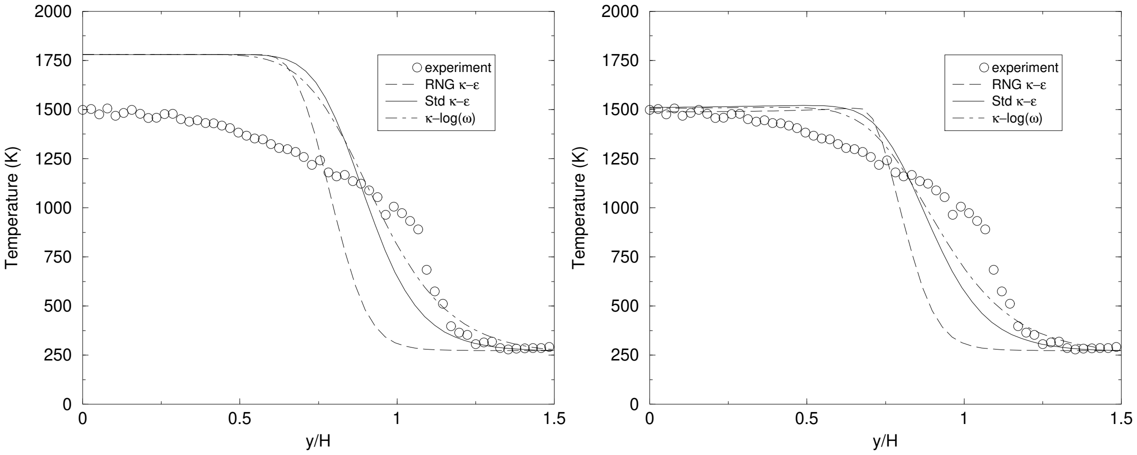

Figure 28: temperature distribution at $x/H = 6.25$: adiabatic model (left); non adiabatic model (right);

2.3 Discussion

2.3.1 Adiabatic model

From the analysis of the pictures shown in the previous section some remarks could be made:

[1] dimension of ricirculating region behind the obstacle

it is strongly underestimated; a remarkable exception is represented by the simulation produced by the RNG $\kappa - \epsilon$ model;

[2] streamlines pattern and velocity fields downstream

profiles of crosswise velocity components far downstream of the obstacle suggest that the streamlines do not bend toward the combustor axis, as found by most of the calculations; again the RNG model gives the correct qualitative behaviour;

[3] temperature level

all models predict a temperature level, right behind the obstacle, given by the adiabatic flame temperature which, as a matter of fact, overestimates of about 500 K the measured level; in reference [1] it is suggested a power loss through the solid bar due to heat conduction; moreover, the temperature measures show a minimum level (about 1250 K) upstream, with respect to about 1500 K downstream, which can be explained only by assuming a certain level of instability of the vorteces behind the obstacle which in turn may allow fresh mixture to be entrained;

[4] flame opening

RNG results determine the least degree of flame opening; the $\kappa - log(\omega)$ results show the maximum level, followed by the standard $\kappa - \epsilon$;

[5] temperature profiles

this issue is tightly connected to the previous one due to the temperature relation to the progress variable: all models fail to reproduce the slope of the temperature profiles; apparently the worst slope is that produced by the RNG model, which is the steepest one: this is in contradiction to the previous comments about the RNG results;

[6] effects of turbulence model

turbulence modelling seems to play a fundamental role for the correct simulation of the ricirculating vorteces and the flame front opening as well;

As reminded previously in the previous chapter, the temperature versus the progress variable relation must also be taken into acount when discussing the results. The TFC model, as in origin developed and implemented into Ares code, is adiabatic and non heat-conducting. The model is adiabatic because, since $T = T(\tilde{c})$, only the progress variable equation is solved, with Neumann wall boundary conditions. As a result, no isothermal wall conditions can ever be used, and the suggested heat loss through the conductiong bar, cannot be simulated. The model is also non heat conducting because there is no way to diffuse internal energy in a stream of burned gases $\tilde{c} = 1$. In other words, a burned stream cannot be cooled, which represents a model limitation.

Whether the heat conduction loss through the walls, or the heat diffusion within the burned stream of gas, or both of them, are responsible for the lower temperatures, the computed density fields are much lower than the measured ones and, as a consequence, the velocity fields are also affected due to the continuity equation. The higher velocity levels might in turn interact with the turbulence model and generate at the end a much smaller ricirculating region. In other words, there is a chain reaction of effects that must be understood. The better behaviour of the RGN turbulence model might, in the end, have been determined by chance only.

2.3.2 Non adiabatic model

The maximum temperature value falls to about 1500 K when using the non adiabatic model, recovering the measured values, apart from the section closest to the obstacle. It ought to be put in evidence here that, even tough isothermal conditions have been used at the obstacle solid walls, in order to take into account the exchange of thermal energy between the main flow and the obstacle itself, this mechanism of energy transfer seems not being sufficient to give reason of the measured temperature drop at the first cross section behind the obstacle. According to [1] it has been experimentally observed that the vortex system downstream the obstacle shows a pulsatile behavior, namely it moves back and forth along the channel axis. This movement could be responsible for the entrapment of gas at lower temperature in the zone right behind the obstacle, which would lead to a lower value of the average temperature. This effect, which is of strongly unsteady nature, has not been accounted for in anyway in the present simulation, which presents only stationary results.

The streamwise velocity component at section $x/H = 1.04167$ doesn't seem to be effected too much by the errors made in the evaluation of the temperature field, showing no significant difference between the results obtained by using the two models. At the two remaining sections further downstream the channel, the effect of the energy diffusion becomes more evident, so that the maximum error made in the evaluation of the velocity is reduced by around 4 to 9 m/s depending on the turbulence model used and on the examined location.

Some improvement in the results could be also observed for the crosswise component of velocity. The most significant effects are found for the standard $\kappa - \epsilon$ model, for which the relative maximum error has been reduced up to about 30%.

As expected, the most relevant improvement on the results are obtained in the evaluation of the temperature field. The maximum level of the temperature is well captured by the model, as well as the flame front position and thickness. Diffusion in the crosswise direction is still poorly evaluated compared to the measures, and might depend upon the turbulence model.

The examination of figures 17, 18 and 9, 25 shows no significant improvement in the resolution of both the turbulent kinetic energy and axial distribution of the longitudinal velocity component, by using the non adiabatic TFC model.

3 Conclusion

In the present work the implementation of the non adiabatic version of the TFC model and its validation have been presented. All the computations have been also carried out by making use of the adiabatic version of the TFC model. The choosen test case, namely the ENSMA combustor, has proven itself to be a very tough one and has represented a good challange for testing the combustion code Ares. The difficulties which have been encountered were related to the TFC combustion model as well as to the turbulence models. The obtained results have shown the accuracy improvement that could be achieved in the computation of the temperature field by making use of the non adiabatic version of the model. The more correct evaluation of the fluid flow temperature has also determined an improvement in the computed velocity profiles. A correct description of the turbulent quantities proved to be an important issue and the RNG $\kappa - \epsilon$ model gave the best results in comparison to both the standard $\kappa - \epsilon$ and the $\kappa - log(\omega)$.

References

[1] *First European Test for Combustion Modelling Workshop*. Aussois, France, February 5-10, 1995.

[2] Fluent Inc. *Fluent 5 User's Guide*. Fluent Inc., 1998.

[3] Chibbaro S. Talice M. and Mulas M. "Validazione del codice ARES". Technical Report CRS4-TECH-REP-02/22, CRS4 Research Centre, z.i. Macchiareddu, strada VI, 09010 Uta (Ca), February 2002.

[4] V. Zimont and M. Barbato. "Premixed and Partially Premixed Turbulent Combustion: Theory and Modelling". Technical Report CRS4-TECH-REP-97/71, CRS4 Research Centre, z.i. Macchiareddu, strada VI, 09010 Uta (Ca), October 1999.

[5] Zimont, V.L., Polifke, W., Bettelini, M. Weisenstein W. An Efficient Computational Model for Premixed Turbulent Combustion at High Reynolds Numbers Based on a Turbulent Flame Speed Closure. *Journal of Engineering for Gas Turbines and Power*, 120, July 1998.